Hindawi
Advances in Civil Engineering
Volume 2023, Article ID 7471721, 16 pages
https://doi.org/10.1155/2023/7471721

Research Article

Two-Stage Caving Characteristics of Complex Irregular Goaf: A Case Study in China

Junyang Zhang[1], **Zonghong Zhou**[1], **Jing Zhang**[1], **Yin Liu**[1,2] and **Yang Liu**[3,4]

[1]*Faculty of Land Resource Engineering, Kunming University of Science and Technology, Kunming 650093, China*
[2]*Heqing Beiya Mining Co., Ltd., Dali 671507, Yunnan, China*
[3]*Department of Resources and Environmental Engineering, Wuhan University of Science and Technology, Wuhan 430081, China*
[4]*Hubei Key Laboratory for Efficient Utilization and Agglomeration of Metallurgic Mineral Resources, Wuhan 430081, China*

Correspondence should be addressed to Jing Zhang; yuanzhongni33@163.com

Received 2 July 2023; Revised 20 September 2023; Accepted 7 October 2023; Published 25 October 2023

Academic Editor: Lei Weng

Different from the goaf formed by normal mining, the goaf formed by the continuous caving of the lower illegal goafs is extremely irregular and unstable, which leads to the difference in the goaf caving characteristics. Taking the complex irregular goaf of the Shirengou Iron Mine in China as the research object, the 3D laser scanning technology is used to detect the goaf shape and analyze the cause of the formation. Then, the caving characteristics of the goaf are analyzed by the methods of the numerical simulation, the monitoring of the crash of the caving rock, and the monitoring of the deformation of the arch foot. The simulation results show that the transverse expansion of the irregular goaf boundary is mainly along the perpendicular to the direction of the ore body strike when the goaf caves upward in the initial stage. Additionally, the monitoring results show that the caving characteristics can be divided into two stages: the paroxysmal caving stage and the periodicity caving stage. The paroxysmal caving characteristics are intense and irregular, while the periodicity caving characteristics have obvious periodicity, which is mainly reflected in the periodic alternation between the mass caving and the temporary stability. The interval period of the goaf mass caving is about 15–30 days and is changed by the progress of filling treatment. The conclusions in this work reveal the particularity of the caving characteristics in the complex irregular goaf and contribute to the improvement of the caving characteristics and the prediction of mass caving.

1. Introduction

The goaf formed by the excavation of the underground ore body, one of the major hidden dangers of mine safety production, easily causes the environmental degradation and the serious waste of mineral resources. Moreover, the complex goaf leads to the deterioration of mining conditions, such as the pillar deformation [1, 2], the difficult maintenance of stope and roadway [3, 4], the rock mass caving [5, 6], and the surface collapse [7, 8], and so on, among which the goaf caving is a common phenomenon in the mining process [9–11]. The caving of the surrounding rock and the air shock waves of the caving block seriously threaten the safety of personnel and equipment [12, 13]. Therefore, the study on the characteristics of goaf caving has the great practical significance.

The goaf volume decreases by the goaf surrounding the rock caving due to the loose coefficient of the rock. Enough caved blocks can effectively prevent the deformation of the goaf surrounding rock [14–16]. However, the continuous upward caving of the surrounding rock of large goaf is easy to cause the surface subsidences [17–22]. Based on the theoretical research and engineering case studies, Ren et al. [23] divided the caving characteristics of the process of surface subsidences into four stages: initial caving, continuous caving, large caving, and lateral caving. The surface easily occurs subsidence when the goaf caving reaches the large caving stage. Therefore, the mechanical model of critical continuous caving of the rock mass was proposed to control the range of the goaf caving [24–27].

The caving of the goaf surrounding rock related to the mining methods, the surrounding rock properties, and the geological environment is a complex physical phenomenon. Singh et al. [28] discussed the effect of mechanical parameters on the roof caving behavior. Sui et al. [29] utilized the

situ measurements to study the influence of the thickness and properties of the overburden on the development of caving. Zhang et al. [12] combined multiple methods such as theoretical analysis, laboratory testing, numerical simulation, and field measurement to accurately calculate the compaction characteristics of a caving zone in longwall goaf. Rezaei [30] suggested the overburden depth has the maximum effect, and the Poisson's ratio has the minimum effect on the caving zone. Lannuzzo [31] suggested the large displacement of rock mass depends on the failure mechanism and the stress state inside the structure. However, the caving characteristics of the surrounding rock are changeable due to the different geological environments. Additionally, most scholars [32–35] assumed the goaf shape is regular to study the caving characteristics due to the hidden of the goaf. Actually, the irregularity of the goaf shape plays an important role in the caving evolution of the surrounding rock. In terms of the goaf shape, the caving characteristic of the regular goaf formed by normal mining is easily summarized by the theoretical model or the numerical simulation. However, the caving characteristics of the complex irregular goaf are difficult to form a general rule due to the complexity of the formation and the difference in engineering problems.

With the development of science and technology, most detection techniques can be used to determine the goaf shape, such as the 3D laser scanning [36, 37], the seismic exploration technique [39, 40], and the measurement of radioactivity [40, 41]. Moreover, the method of combining the detection results and numerical simulation contributes to the study of the caving characteristics [42, 43]. Certainly, the monitoring is also a practical approach to mastering the caving law of goaf surrounding rock, such as the stress monitoring [44, 45], the microseismic monitoring [46, 47], and the acoustic emission monitoring [48, 49]. In the joint monitoring aspects, the stress monitoring and microseismic or acoustic emission are always combined to estimate the goaf failure [50, 51]. Additionally, Fan et al. [52] proposed the combination of the interferometric synthetic aperture radar technique and the probability integral model to invert the goaf characteristics.

In the following sections, a complex irregular goaf of the Shirengou Iron Mine in China is taken as the research object to analyze the general caving characteristics. The cause of the formation can be preliminarily concluded by the 3D laser scanning technology. Then, the discrete element software 3DEC is used to simulate the caving process in the initial formation stage, which helps to preliminarily master the goaf caving characteristics. Based on a combination of the monitoring of the crash of caving rock and the deformation of the arch foot, the two-stage caving characteristics are summarized, which reflect the particularity of the goaf in this work and provide a reference for the general caving characteristics of the complex irregular goaf.

2. Engineering Background

The Shirengou Iron Mine is an Anshan-type magnetite deposit. As shown in Figure 1, the open-pit mining is applied to the mine deposit above 0 m level, the shallow hole shrinkage mining method is applied to the mine deposit at 0 to −60 m level, and the sublevel open stoping with subsequent filling method is applied to the mine deposit below −60 m level. The level above −210 m is the scope of the mining rights of the mine. In the mining area of −60 to −210 m level, the length of the panel arranged along the strike of the ore body is 100 m, the stage height is 90 m, the sublevel height is 15 m, and the room width is 20 m. The auxiliary middle section is set with a height of 45 m to meet the mine ventilation and production safety.

As shown in Figure 1, the mine has M1, M2, and M3 ore veins. The M2 ore vein, a steeply inclined thick ore body with the 15–20 m thickness and 50°–70° dip angle, is the main ore body currently. On May 31, 2019, the roof of the illegal goaf under the −210 m level suddenly caves to the main production level (−210 m level). Then, the height and width of the caving goaf (called the M2 goaf in this paper) increase continually and quickly caves to the −165 m level. To meet the demand for filling slurry required for mine production, the filling slurry used for the goaf treatment is limited, with only 30,000 m^3 per month. Therefore, the site of goaf treatment is characterized by falling while caving.

According to the site of the M2 goaf detection (Figure 2(a)), the visibility of the detection environment is low. Therefore, the detection method of the 3D laser scanning coupled with the defogging is adopted to detect the goaf morphology. The demisting is carried out before the detection, mainly to improve the detection environment. As shown in Figure 2(b), the probe is fed into the goaf with the connecting rod so that the goaf morphology can be detected in the drift.

The detection results (Figure 3) show that the M2 goaf inclined from north to south is extremely irregular. The clearance height of the M2 goaf is about 120 m, the maximum width along the strike direction of the ore body is about 102 m, and the maximum width of the vertical strike direction of the ore body is about 98 m. Meanwhile, in the north of the M2 goaf, there are four illegal goafs (PG-01 goaf, PG-02 goaf, PG-03 goaf, and PG-04 goaf) of different sizes with a large distribution range, which certainly affect the development of the M2 goaf boundary in the direction of ore body. This may be the main reason why the M2 gsaf expands greatly upward at the early stage of formation and develops in the width direction.

The results of the field investigation show that the type of the surrounding goafs is illegal. Generally, the illegal mining personnel are mostly the people around the mining area, and the mining methods are the room-and-pillar method and the irregular shallow hole shrinkage mining method. Therefore, the characteristics of the remaining goaf are lower height, irregular, large distribution, and more layers. As shown in Figure 3, the maximum height of the illegal goaf is less than 45 m according to the statistics of the height of the surrounding goafs. Considering that the clearance height of the M2 goaf is about 120 m, it can be preliminarily inferred that the formation of the M2 goaf is caused by the caving of the lower multilayer illegal goaf continuously.

The cross sections of M2 goaf in the production levels are shown in Figure 4. The lower illegal goafs first cave to the T-drift 10# at the −210 m level and quickly cave to the −165 m

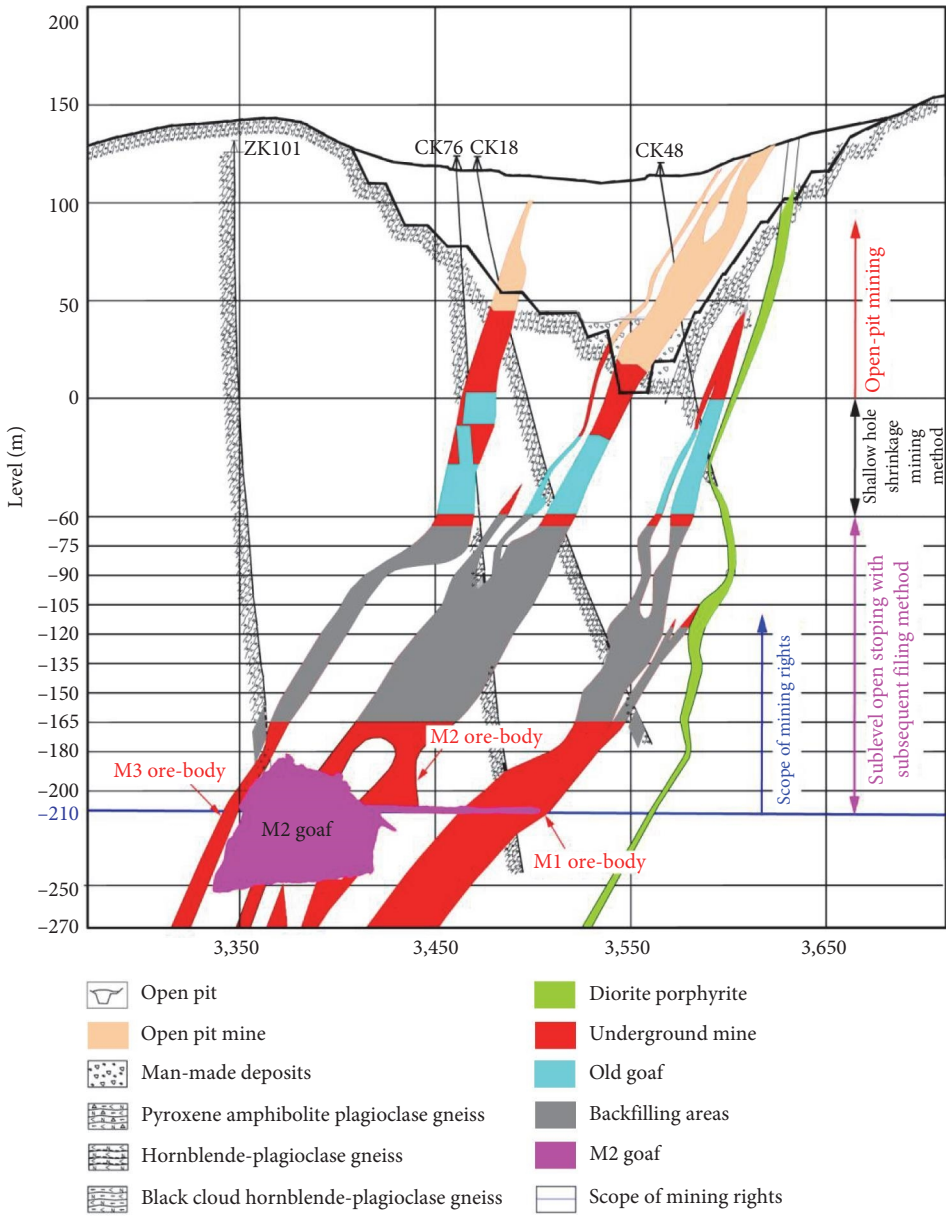

Figure 1: Profile of 10# exploration line in the Shirengou Iron Mine.

level. It can be seen from the layout of mining engineering in Figure 4 that the ore bodies above −165 m have been mined, and the ore bodies in the area of −165 to −210 m are currently being mined. Additionally, the goaf shapes of the cross sections are located in the main production area. Moreover, the cross sections are different, and the boundaries of the cross sections are relatively irregular, which show that the caving activities will continue and the boundaries will further expand. The continuous caving of the M2 goaf has a great impact on the safety management of the goaf and the safety mining of the surrounding ore bodies.

3. Paroxysmal Caving Characteristics

3.1. Model and Parameters. During the initial stage of the formation of the M2 goaf, the caving activity of the goaf surrounding rock is intense and frequent. The surrounding rock on the north side of the M2 goaf is more unstable than the south side due to the shape of the caving goaf and the distribution of the surrounding goafs. Therefore, the goaf model can be established according to the right view of the caving goaf (Figure 3(c)). The ore-rock distribution characteristics refer to the profile of 10# exploration line of the Shirengou Iron Mine (Figure 1). As shown in Figure 5, the final numerical model size (length × width × height) is 560 m × 600 m × 553 m. The x-axis is perpendicular to the y-axis, that is, the strike direction of the ore bodies. The dip direction angle and dip angle of the fault at the −195 m level are 115° and 14°, respectively.

According to the mining data, the ore bodies above 0 m level are the remaining ore body by the mining from open pit to underground, the ore bodies of the 0 to −60 m level are

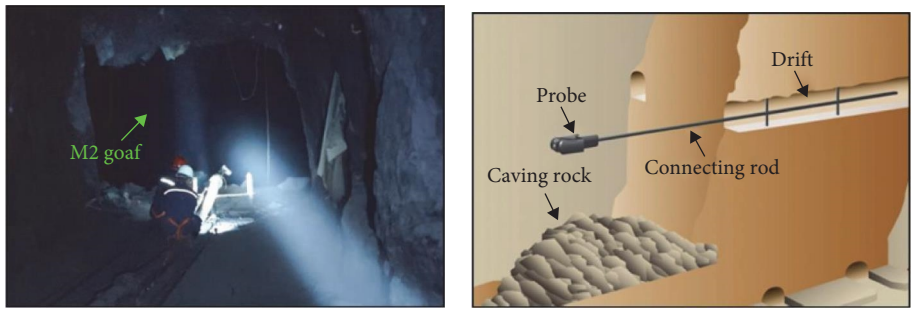

Figure 2: Scene diagram of 3D laser scanning: (a) detection site; (b) schematic diagram.

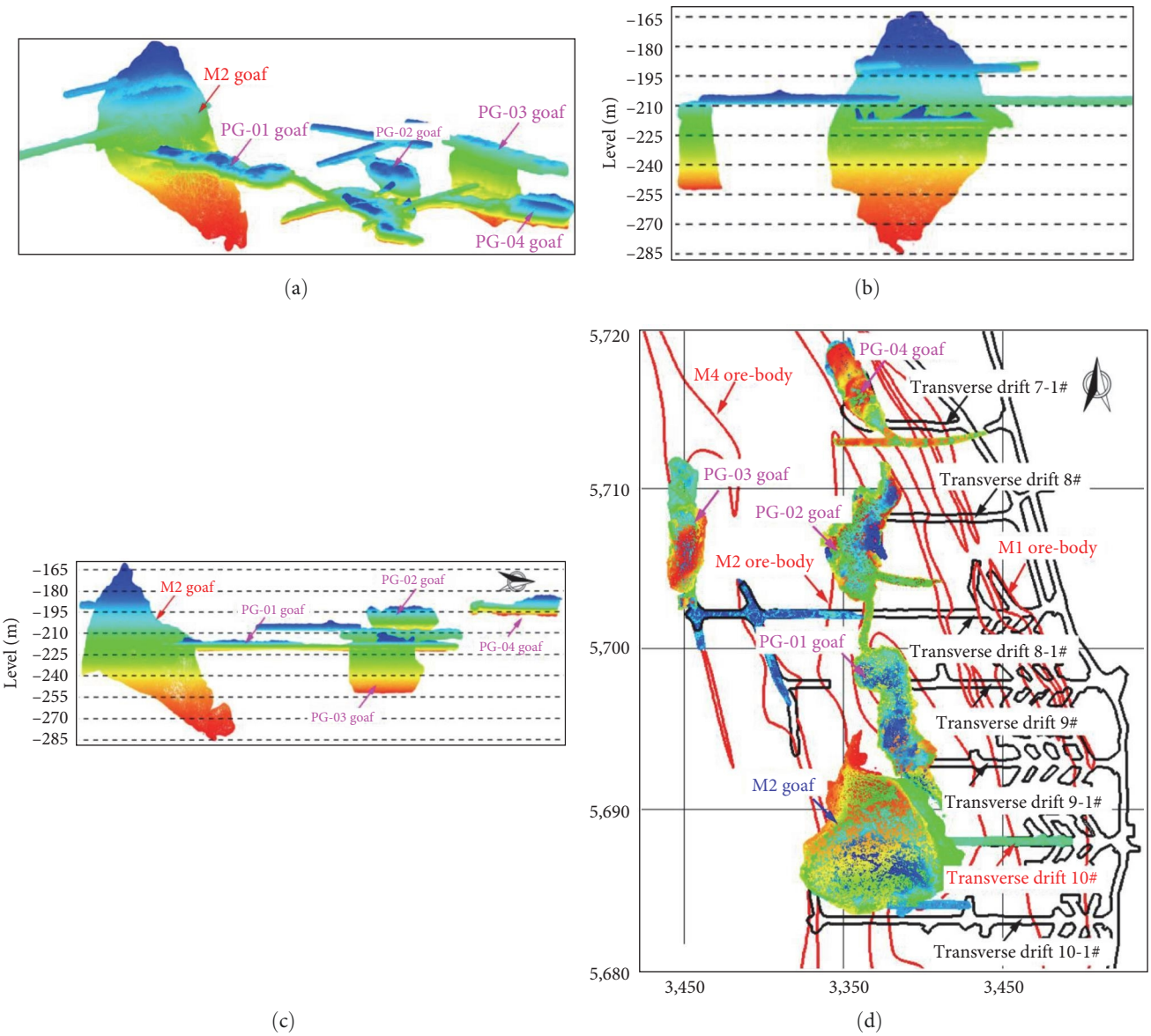

Figure 3: Detection result for M2 goaf and its surrounding goafs: (a) perspective; (b) front view; (c) right view; (d) top view.

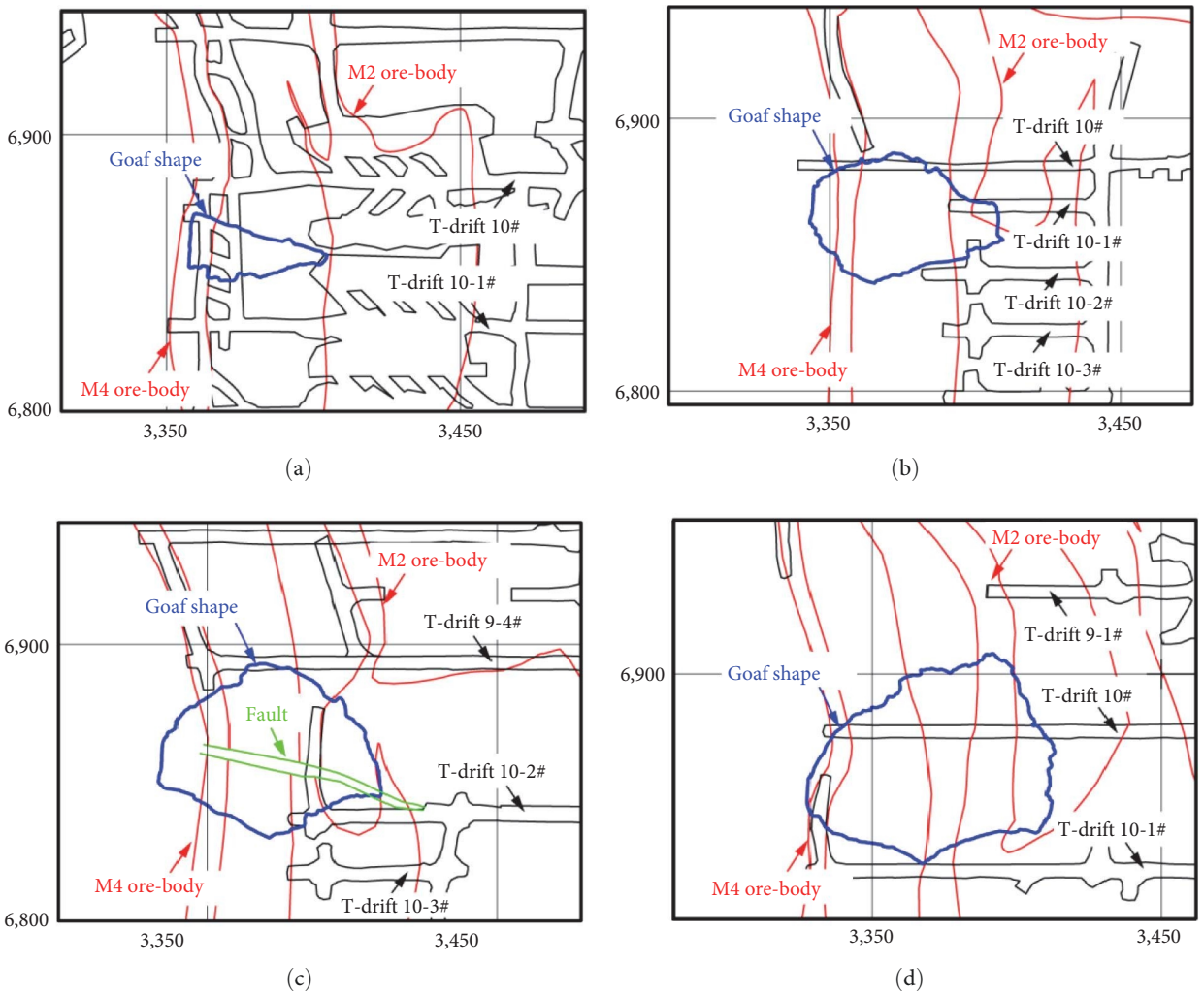

Figure 4: Cross-sections of M2 goaf in the production levels: (a) −165 m level; (b) −180 m level; (c) −195 m level; (d) −210 m level.

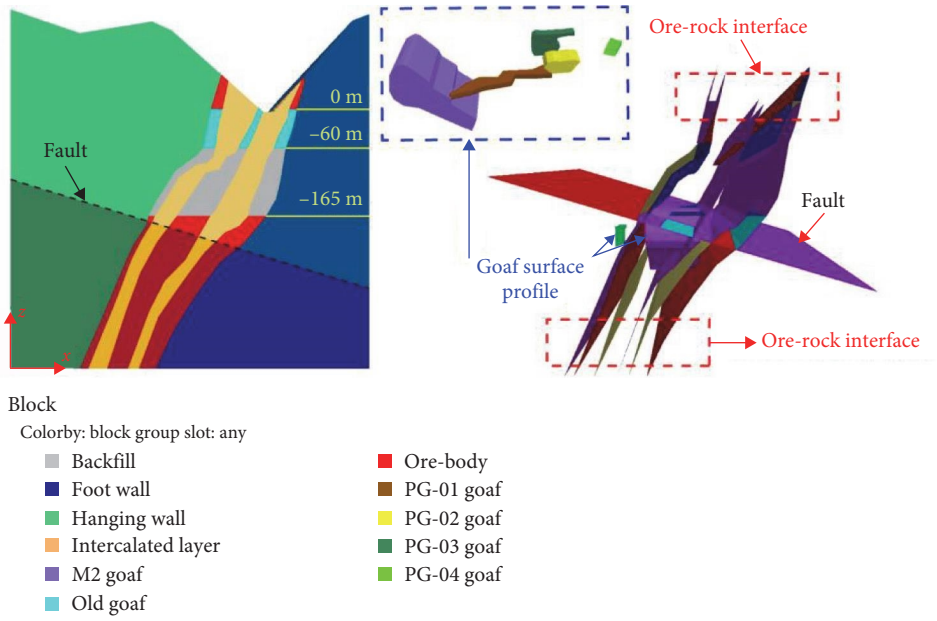

Figure 5: Numerical model for the paroxysmal caving.

Table 1: Rock mass physical and mechanical parameters.

Type	Density (kg m^{-3})	Tensile strength (MPa)	Elastic modulus (GPa)	Poisson's ratio	Volume modulus (GPa)	Shear modulus (GPa)	Friction angle (°)	Cohesion (MPa)
Hanging wall	2,720	0.70	6.45	0.23	3.98	2.62	44.36	2.34
Ore-body	3,570	0.52	11.87	0.22	7.07	4.86	38.98	3.87
Foot wall	2,730	1.21	9.32	0.24	5.97	3.76	54.28	3.64
Intercalated layer	2,830	0.79	7.56	0.26	5.25	3.00	46.35	3.32
Backfill	2,300	0.52	2.08	0.28	1.58	0.81	28.53	1.41
Old goaf	2,000	0.27	1.42	0.31	0.24	0.10	31.42	0.98

Table 2: Structural plane mechanical parameters.

Type	Normal stiffness (GPa)	Tangential stiffness (GPa)	Tensile strength (MPa)	Friction angle (°)	Cohesion (MPa)
Interlayer joint	9.54	6.48	0.24	22.37	1.59
Fault	3.39	2.90	0.17	27.22	1.13

formed by the shallow hole shrinkage mining method, and ore bodies below −60 m level are mind by the sublevel open stoping with the subsequent filling method. Through the application of different mining methods, a large amount of goaf remains at the 0 to −60 m level, which can be named old goafs in Figure 5. Considering that the area of the 0 to −60 m level has been mined for a long time, the investigated area is limited. Therefore, the physical and mechanical parameters of the old goaf can only be estimated through the local partial field investigation and point load test. The rock mass among the ore bodies can be called the intercalated layer. In the level of −60 to −165 m, the ore bodies mined by the sublevel open stoping with the subsequent filling method are named the backfill. Mechanical parameters of rock masses and structural planes (as shown in Tables 1 and 2) are obtained according to the geological conditions, the field investigation, and the laboratory tests. The elastic stiffness and friction characteristics of the structural plane are included in the numerical model, which accords with the basic characteristics of rock mass.

The constitution model for the numerical calculation is the Mohr–Coulomb criterion. The boundary conditions of the numerical model are the displacement boundary conditions: (1) the left and right boundaries of the model are fixed at $x = 0$ and $x = 560$ m to limit the velocity in the x direction, (2) the front and back boundaries of the model are fixed at $y = -170$ m and $y = 430$ m to limit the velocity in the y direction, (3) the bottom boundary of the model is fixed at $z = -400$ m, and (4) the top boundary of the model is a free surface.

3.2. Results. The gravity stress and mining stress are considered in the numerical calculation. The pore water pressure is ignored due to the simple hydrogeological conditions in the Shirengou Iron Mine. When the numerical model reaches the initial stress equilibrium under the condition of gravity stress, the goafs start to excavate in a certain sequence. The excavation sequence of the goafs is (1) M2 goaf, (2) PG-01 goaf, (3) PG-02 goaf, (4) PG-03 goaf, and (5) PG-04 goaf.

As shown in Figure 6, the surrounding rock of M2 goaf on a large scale includes the hanging wall, the ore body, the footwall, and the backfill. Therefore, the numerical simulation results selected by the different plane directions are slightly different. The plane with the normal direction (1, 0, 0) and the coordinate point (250, 0, 280) is selected to observe the caving and fracture propagation of the M2 goaf surrounding rock. The simulation results (as shown in Figure 6) show that the surrounding rock of the M2 goaf gradually becomes unstable with the expansion of existing fractures and the development of new fractures in the goaf surrounding rock. The surrounding rock is prone to caving when the fractures are connected with each other. The final caving curve of M2 goaf is an approximate arch shape, which indicates the M2 goaf surrounding rock achieves the stress balance state under the condition of continuous excavation.

As shown in Figure 7, when the PG-01 goaf is excavated, the M2 goaf surrounding rocks in the −165 to −210 m level have a relatively large caving range. However, only the M2 goaf surrounding rock in the −165 m level occurs during the caving when the PG-02 goaf is excavated, and the transverse caving ranges of M2 goaf in the −165 to −210 m level are unchanged when the PG-03 goaf and the PG-04 goaf are excavated. The simulation results show that the PG-01 goaf and PG-02 goaf have a great impact on the caving of M2 goaf surrounding rock due to the closer distance. Moreover, the lower of the M2 goaf is easy to achieve stability. Additionally, the maximum transverse caving range of M2 goaf in the −165 to −210 m level is 48.31, 41.23, 36.75, and 45.32 m, respectively. Meanwhile, the goaf roof caves on the 130 m level, and the goaf area in the −165 to −210 m level increases by 2.23 times, which indicates the caving range is large in the paroxysmal caving stage.

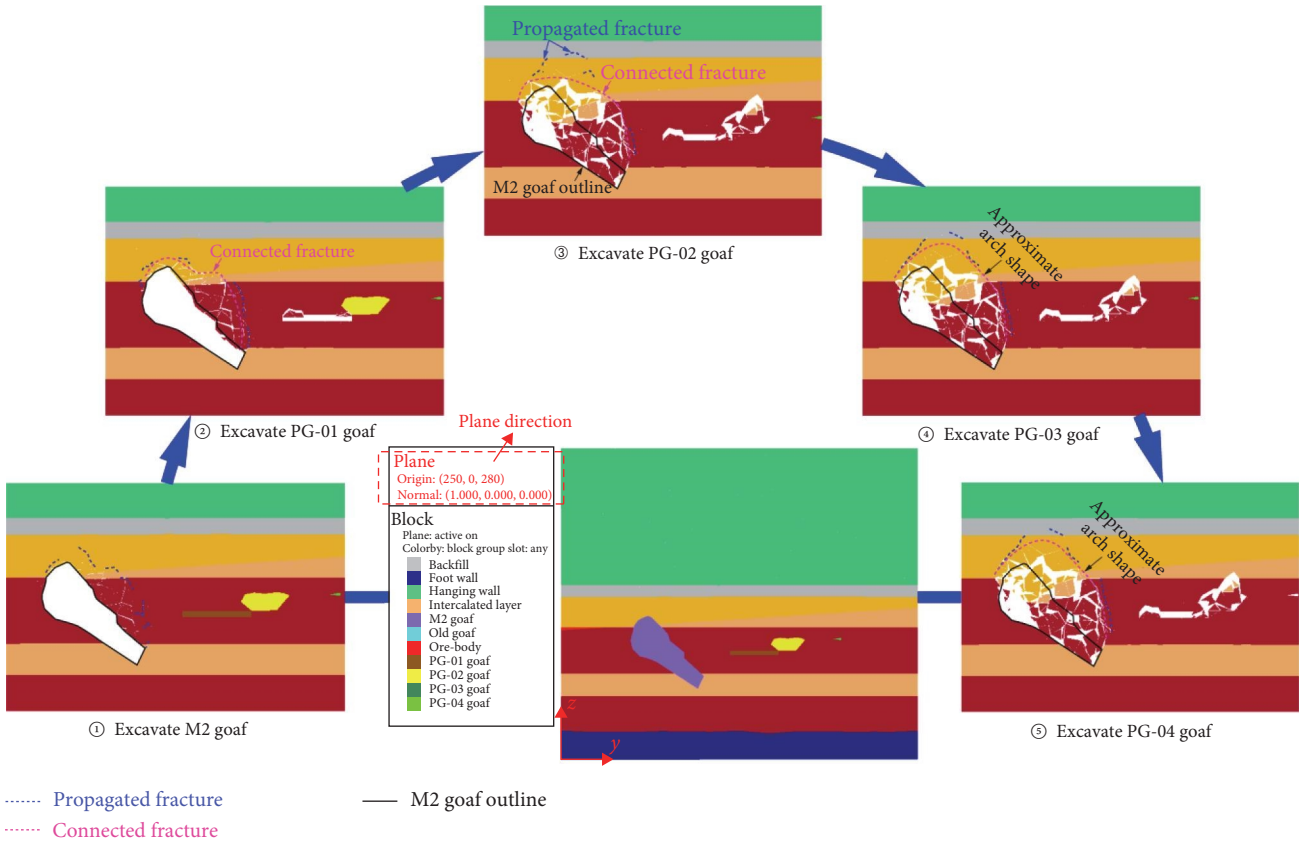

Figure 6: Fracture development along the direction of the ore body strike.

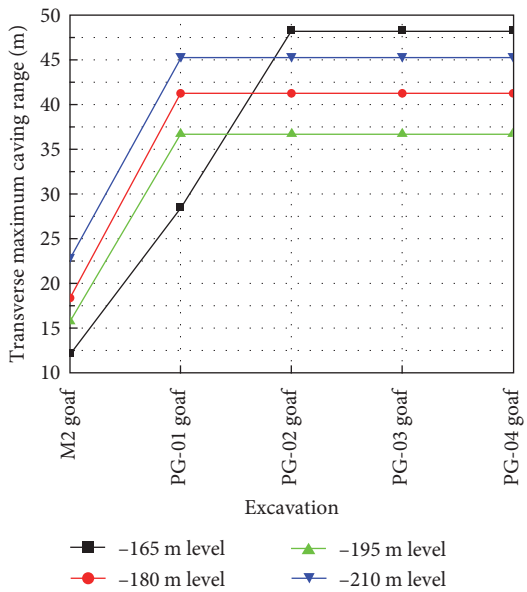

Figure 7: Statistics of the maximum transverse caving range of the M2 goaf.

3.3. Monitoring the Crash of Caving Rock. Effectively, the monitor may be adopted to recognize the degree of goaf caving and prevent goaf hazardous accidents. Ordinarily, microseismic monitoring and acoustic emission monitoring can predict the occurrence of goaf caving. However, M2 goaf caving is an inevitable event, and the frequency of goaf caving is high in the paroxysmal caving stage. The prediction of the caving range and the classification of goaf caving are the key to prevent goaf hazardous accidents. Clearly, the previously mentioned monitoring methods are not only expensive but also difficult to achieve the target.

The field investigation shows that the crash of caving rock included smaller sounds and louder sounds, which can be distinguished by the volume, frequency, and duration. Considering that the scale of M2 goaf is relatively large and the frequency of goaf caving is relatively frequent, the crash sound of caving rock is easy to monitor due to the large scale of the M2 goaf. The main human error in the monitoring is the interference of underground blasting sound. However, the difference between the crash of caving rock and the blasting sound is significant. The smaller crash sound is clear and loud and mostly occurs intermittently with a short duration, which is different from the dullness of the underground blasting sound. It can be used to characterize the sporadic caving of the goaf surrounding rock. The louder crash sound, accompanied by the paroxysmal boom of high and low is dull, rich, and loud. The average time of a louder crash sound is about 5 min, which is quite different from the duration of the underground blasting sound. It can be used to characterize the mass caving of the goaf surrounding rock. Therefore, the monitoring of the crash of caving rock, an economical

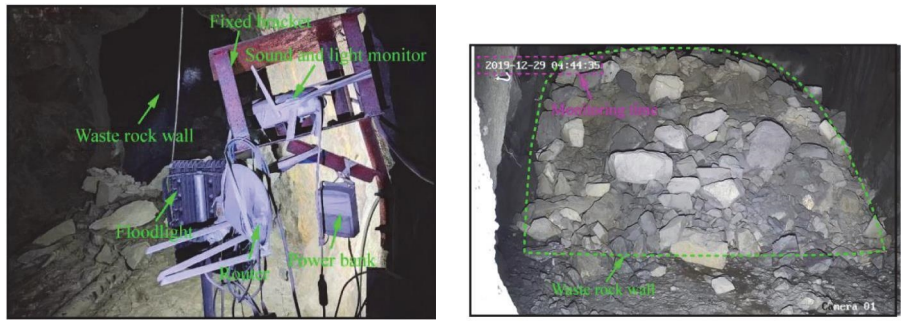

(a) (b)

Figure 8: Monitoring equipment of the goaf rock caving sound: (a) monitoring equipment; (b) screenshot of recording video.

and reasonable monitoring method, can be introduced to recognize the degree of goaf caving.

As shown in Figure 8, the monitoring equipment includes the sound and light monitor, the router, the power bank, the floodlight, and the waste rock wall. The sound and light monitor is applied to monitor and record the sound of the caving rock crash, the goaf bottom. The router, the power bank, and the floodlight are used to provide the network, power, and lighting, respectively. The waste rock wall is used to prevent the impact of airflow induced by the goaf caving and protect the safety of monitoring equipment. It is worth noting that a space of 1 m reserved between the top of the waste rock wall and the roadway is to observe the airflow from the top of the waste rock wall.

Considering that the T-drift 10-2# at the −195 m level (Figure 4) is connected to the M2 goaf, the monitoring point is set in the drift. Moreover, the monitoring point can also observe the development of the fault in the −195 m level. The monitoring equipment is fixed on the drift wall, and the sound and light monitor is set in front of the waste rock wall. This way, the crash of caving rock behind the waste rock wall can be monitored by the monitor.

The mine arranges professional personnel to analyze the recording videos every day and record the crash index, including the total time of the caving rock, crash, time of the louder crash of caving rock, the average duration of each caving rock crash, and average daily duration of the caving rock crash. The recording videos show that a large turbid airflow appears in the top of the waste rock wall when the sound is louder than the crash of caving rock, which indicates the crash index can characterize the mass caving of goaf surrounding rock.

The monitoring results from July 16, 2019 to January 20, 2020 are shown in Figure 9. The goaf caving occurred frequently from July 16, 2019 to December 10, 2019, and lasted for a long time each day, which is related to the goaf characteristics and complex geological environment. This stage can be called the paroxysmal caving stage due to the suddenness and persistence of caving. In this stage, the louder crash of caving rock occurs continuously. However, the caving frequency is decreasing on the whole. The caving phenomenon shows that the goaf surrounding rock is in an extremely unstable state during the M2 goaf initial formation. The goaf gradually becomes stable with the establishment of stress equilibrium in the surrounding rock. This trend is consistent with the results of numerical simulation (Figure 6).

From December 10 to 28, 2019, the type of goaf caving is sporadic caving, and the frequency of goaf caving is lower. It can be considered that the M2 goaf achieves stability in the process of constantly establishing a new stress balance. However, the crash of Caving Rock appeared again on December 29, 2019. Meanwhile, the number of the louder crash sounds is eight times (as shown in Figure 9(b)), and the average daily duration of the caving rock crash is increasing significantly (as shown in Figure 9(d)). The results show that the stability of the M2 goaf is temporary, and the mass caving of goaf surrounding rock occurs again under the induction of some reason.

4. Periodicity Caving Characteristics

According to the field investigation, the goaf arch foot at the T-drift 10-2# at the −195 m level was seriously damaged on December 26, 2019 (as shown in Figure 10). Subsequently, the louder crash of the caving rock was monitored on December 29, 2019. Therefore, the change in the monitoring data on December 29, 2019, may be related to the failure of the goaf arch foot.

4.1. Caving Arch Mechanical Model. The exposed area of the goaf gradually increases when the ore body is mined according to a mining design. The stress in the goaf surrounding rock exceeds the rock mass strength under the influence of the gravity stress, mining stress, goaf span, and so on. Then, as shown in Figure 11(a), the goaf surrounding rock occurs initially caving and continues caving upward with the expansion of existing fractures and the development of new fractures in the goaf surrounding rock. The final caving arch formed by the stress balance is relatively stable. However, the stable state can easily be disrupted by an inducement, such as the increase of goaf span, the stress concentration, mining stress, and so on. As for the M2 goaf, the reason for the weakened mechanical properties of the arch foundation cannot be ignored due to the undiscovered illegal goaf. Therefore, the failure of the goaf arch foot is possible to cause the mass caving of the goaf surrounding rock.

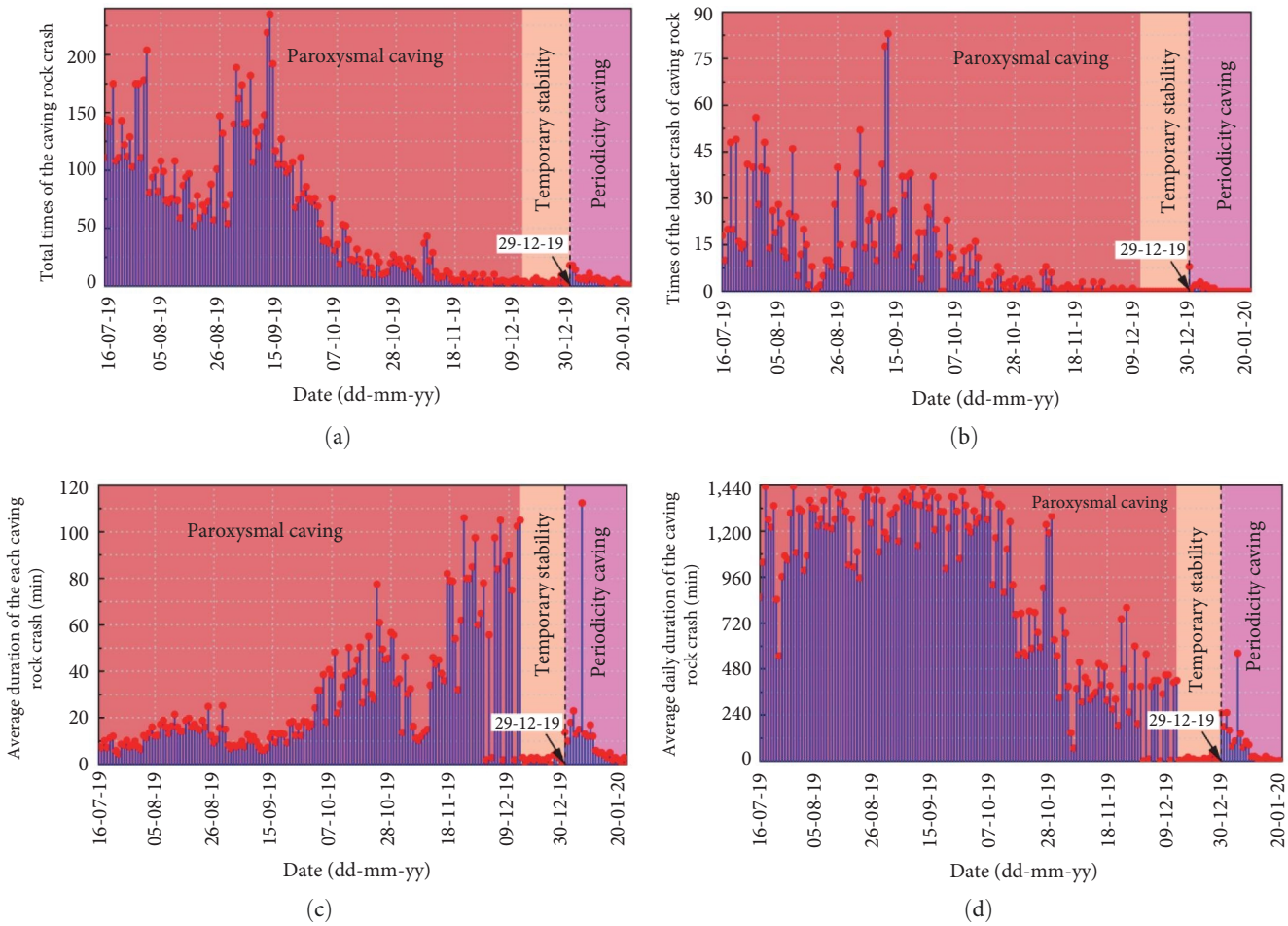

FIGURE 9: Monitoring results from July 16, 2019 to January 20, 2020: (a) total times of the caving rock crash (daily cumulative value); (b) times of the louder crash of caving rock (daily cumulative value); (c) average duration of each caving rock crash; (d) average daily duration of the caving rock crash.

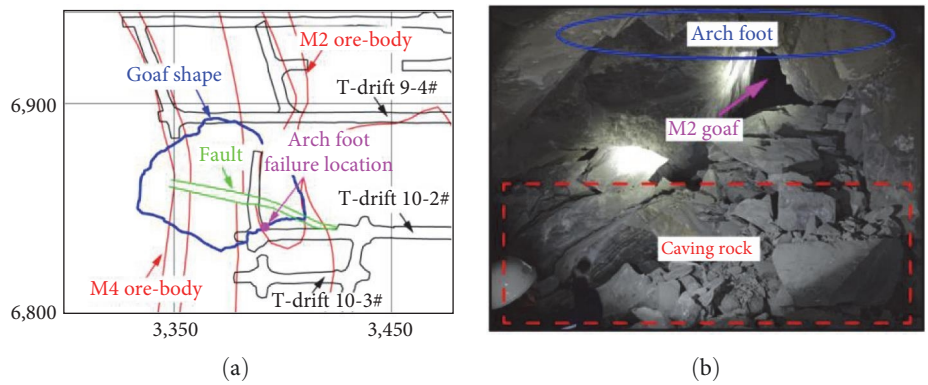

FIGURE 10: Arch foot failure of the caving goaf at the −195 m level: (a) location of arch foot failure; (b) site diagram of arch foot failure.

A mechanical model of a caving arch considering the arch foot pressure can be established to explain the relationship between the arch foot failure and the mass caving. As shown in Figure 11(b), the gravity stress γH is distributed above the caving arch, and the linearly distributed horizontal stress is distributed on both sides of the arch. The ratio of horizontal stress and gravity stress is γ. Assuming that the arch foot pressure F is not perpendicular, it can be decomposed into the horizontal pressure F_1 and the vertical support F_2. Taking the right half arch OM as the research object, the moment equilibrium at the point $M(x, y)$ can be expressed as follows:

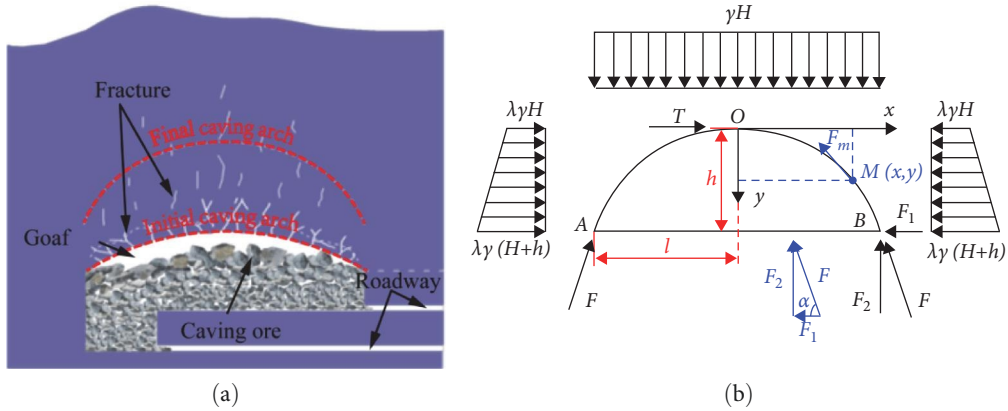

FIGURE 11: Mechanical model of caving arch considering the arch foot pressure: (a) diagram of goaf roof caving; (b) diagram of the force of the caving crash.

$$Ty - \frac{\gamma H x^2}{2} - \left[\frac{\lambda\gamma H}{3} + \frac{\lambda\gamma(H+y)}{6}\right] y^2 = 0, \tag{1}$$

where the parameters H, γ, and λ are the goaf depth, the bulk density, and the lateral pressure coefficient, respectively.

From the force system equilibrium for the right half arch OM as follows:

$$T - F_1 - \frac{\lambda\gamma(2Hh + h^2)}{2} = 0, \tag{2}$$

$$\gamma Hl - F_2 = 0, \tag{3}$$

where the parameters l and h are the half-span and height of the caving arch, respectively.

Set $x = l$ and $y = h$ and combine Equations (1) and (2) to obtain as follows:

$$2\lambda\gamma h^3 + 3\lambda\gamma Hh^2 + 6F_1 h - 3\gamma Hl^2 = 0. \tag{4}$$

Rearranging Equation (4) yields

$$l = \sqrt{\frac{2F_1 h}{\gamma H} + \lambda h^2 + \frac{2\lambda h^3}{3H}}. \tag{5}$$

It can be seen from Equation (5) that the height of the caving arch h increases with the parameter l. Therefore, the increase of the span can cause the further upward caving of the goaf. Moreover, the parameter h is inversely proportional to the horizontal pressure F_1 when other parameters are constant, which indicates the angle α between the arch foot and the horizontal line increases with the height of the caving arch.

As shown in Figure 12, the arch foot pressure F is perpendicular when the caving arch achieves the limit equilibrium arch. Meanwhile, the stress concentration at the arch foot achieves the lowest degree. However, the caving arch for the extremely irregular goaf is not an ideal elliptical arch. The degree of stress concentration in the surrounding rock is large due to the irregularity of the M2 goaf. Therefore, the stress concentration is also the inducement for the destruction of temporary stability (as shown in Figure 9) of the M2 goaf. Additionally, the distribution of lower illegal goaf cannot be clearly detected due to the limitation of the range of mining rights (above the −210 m level). Then, the mechanical properties of the arch foundation can be weakened by the undiscovered illegal goaf upward caving. As a result, the goaf caving occurs again due to the failure of the arch foundation.

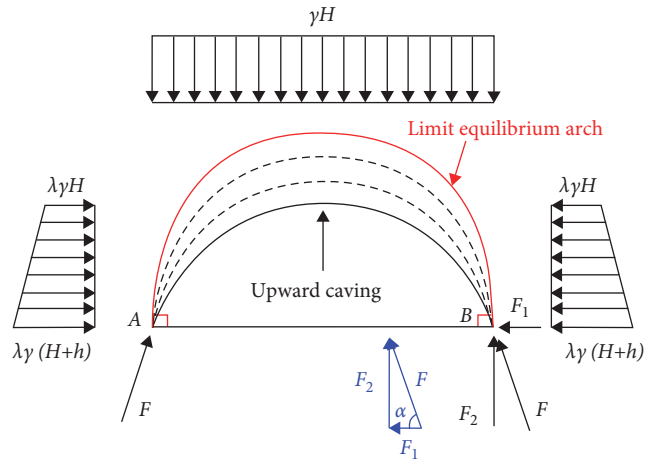

FIGURE 12: Schematic diagram for the change of goaf caving arch.

4.2. Monitoring the Deformation of Arch Foot. The caving arch mechanical model indicates that the failure of the arch foot can cause the surrounding rock of the goaf upward caving. Recall that the caving characteristics in the paroxysmal caving stage, the boundary of the M2 goaf could expand further along the direction of the ore body strike. However, the boundary could extend along the direction perpendicular to the ore body strike from the field caving phenomenon in Figure 10. Coupled with the stress concentration due to the irregular shape of M2 goaf, the mass caving could be occurred along the direction perpendicular to the ore body strike. Therefore, it is necessary to monitor the deformation of the arch foot along the direction perpendicular to the ore body strike.

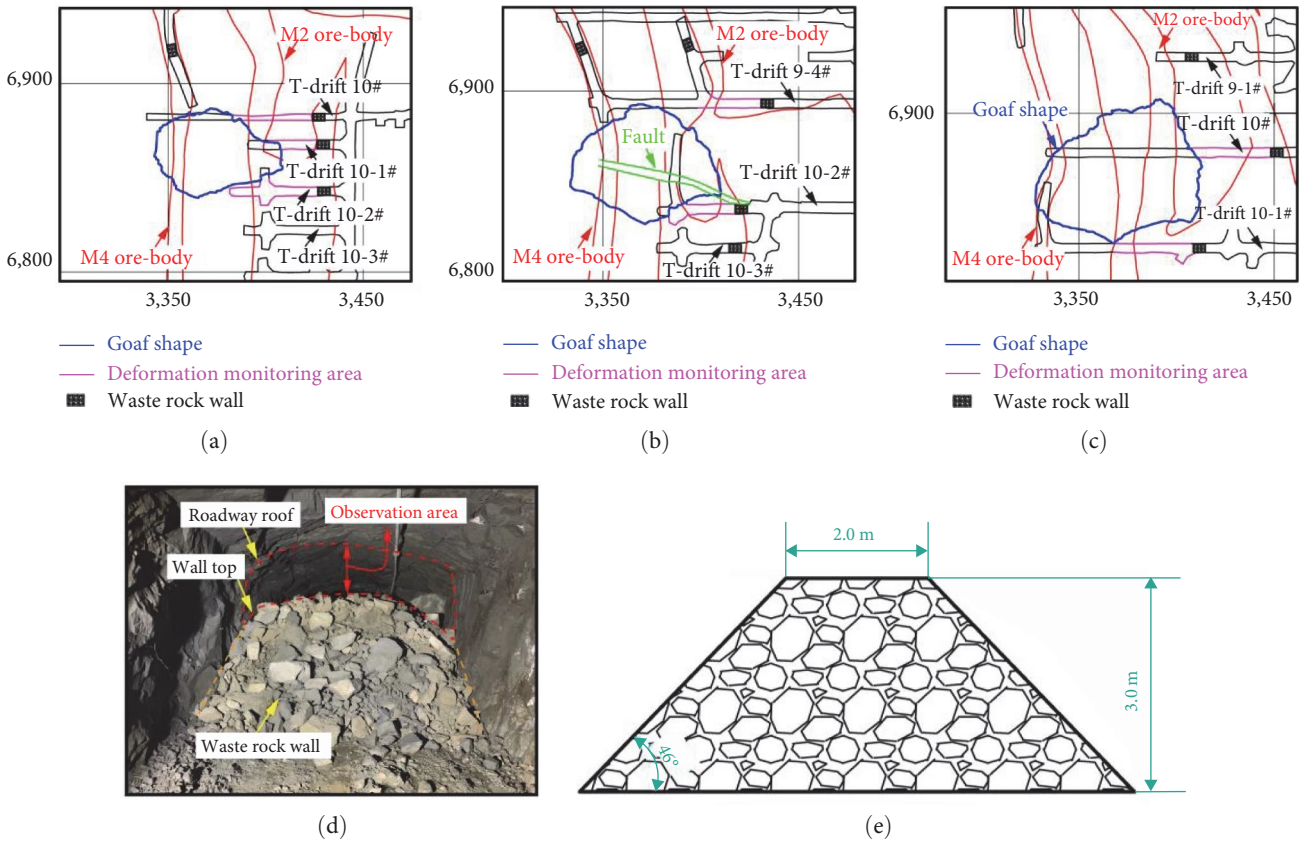

Figure 13: Deformation monitoring of the arch foot: (a) −180 m level; (b) −195 m level; (c) −210 m level; (d) site map of waste rock wall; (e) right view of waste rock wall.

As shown in Figure 13, the deformation monitoring of the arch foot is used to master the expansion of the goaf boundary. In fact, the arch foot of the M2 goaf is below the −210 m level. However, the deformation monitoring of the actual arch foot cannot be monitored due to the lack of development and mining projects in this area. Therefore, the production levels of −180, −195, and −210 m are selected for the monitoring area of the arch foot. The change in the caving arch can be analyzed by the temporary monitoring data.

The monitoring areas select the roadway connected to the M2 goaf and located behind the waste rock wall. In the deformation monitoring of the arch foot, the reserved area between the top of the waste rock wall and the roadway is to observe the deformation of the arch foot. Considering that the deformation of the arch foot is a macroscopic failure phenomenon, the laser finder can be selected to obtain the monitoring data. However, the monitoring personnel must use a reserved area for monitoring to ensure the safety of personnel and equipment.

The field investigation shows that the expansion of the M2 goaf boundary along the perpendicular to the direction of the ore body strike is not obvious in the paroxysmal caving stage. Recall that the activity of goaf caving is intense in the paroxysmal caving stage, which indicates the transverse expansion in this stage is mainly along the direction of the ore body strike. However, the goaf arch foot in the T-drift 10-2# at the −195 m level is seriously damaged when the temporary stability (as shown in Figure 9) is broken. This phenomenon indicates that the goaf boundary begins to expand along the perpendicular to the direction of the ore body strike.

As shown in Figure 14, the general law of the goaf caving after the paroxysmal caving stage can be analyzed by combining with the failure of the arch foot and the louder crash of the caving rock. The period from the data of the goaf formation to December 10, 2019, can be called the paroxysmal caving stage. Then, the temporary stability stage from December 10, 2019 to December 29, 2019 is formed after the paroxysmal caving stage. On December 29, 2019, the goaf mass caving, accompanied by a louder crash sound, occured again.

Recall that the louder crash of caving rock can be used to characterize the mass caving of goaf surrounding rock. As shown in Figure 4, the mass caving and the temporary stability of the M2 goaf change periodically alternately. The interval period of the goaf mass caving is about 15–30 days, and the interval increases with the continuous filling treatment. In this stage, the periodic characteristics of mass caving in the goaf are obvious, which can be considered as the periodic changes of continuous stability and instability of the caving arch. Therefore, this stage can be called the periodicity caving stage.

In the periodicity caving stage, the failure of the arch foot in the deformation monitoring area occurs before the mass

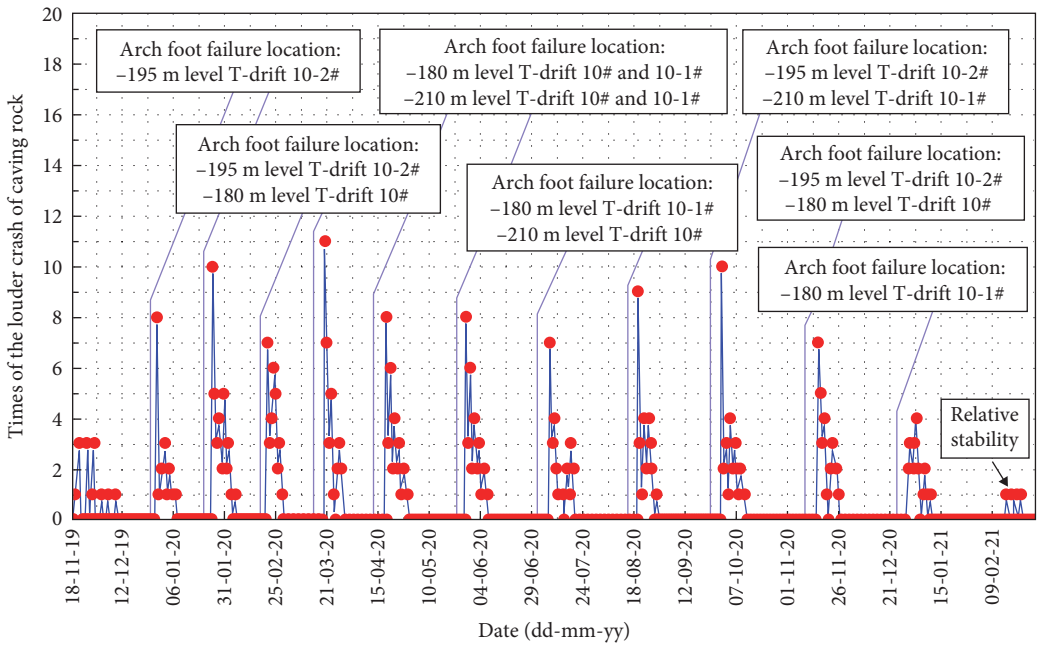

Figure 14: Statistics of the failure of arch foot and the louder crash of caving rock.

caving of the goaf surrounding rock. The lag time for the goaf mass caving is about 3–8 days, which indicates the failure of the arch foot can cause the goaf mass caving. In fact, the support provided by the backfill to the goaf surrounding rock below the −210 m level is the limit due to the slow filling speed. Therefore, the goaf surrounding rock above the −210 m level is easily affected by the failure of the arch foot. However, the stability of the caving arch formed in each cycle is better when the transverse support provided by the backfill stabilizes the arch foundation with the continuous filling treatment. Then, the arch foot is not easy to be damaged. This is the reason for the difference in the cycle and the lag time of the goaf mass caving.

5. Discussions

The two-stage caving characteristics of the M2 goaf show that the surrounding rock caving always exists in the process of filling treatment, which is consistent with the detection results of the 3D laser scanning (Figure 15). As shown in Figure 15, the 3D laser scanning of the M2 goaf has been performed only three times due to the limitations of the production and filling treatment site conditions. The volume of the M2 goaf on March 17, 2021 (216,900 m^3) is close to that on July 22, 2019 (245,000 m^3). However, a total of 498,800 m^3 of filling slurry has been filled into the M2 goaf during the period, which indicates the illegal goaf below the −210 m level is multilayer and numerous. The lower surrounding rock of the M2 goaf gradually enters a stable state under the support of the caving rock and the filling slurry.

Considering that the level above −210 m is the scope of the mining rights of the mine, the comparative analysis of the boundary extension of the M2 goaf in the main production level can better illustrate the two-stage caving characteristics of the M2 goaf. As shown in Figure 16, the boundary of the

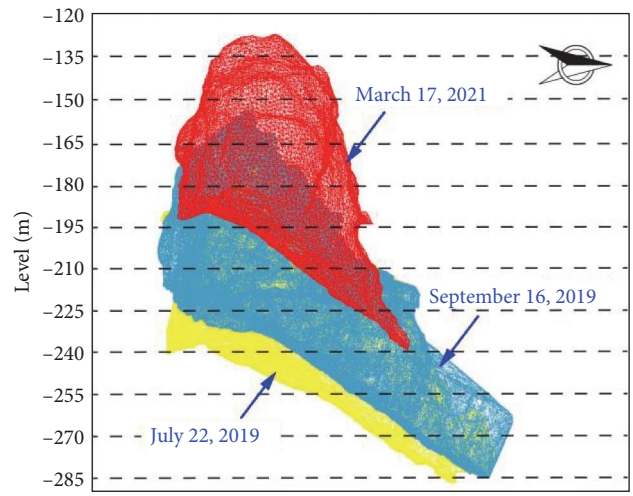

Figure 15: Comparison of the right view of the M2 goaf detection.

M2 goaf in the main production level expanded mainly along the ore body strike direction from July 22, 2019 to September 16, 2019. Meanwhile, the boundary of the M2 goaf in the −180 m level is most obvious, which creates favorable conditions for the paroxysmal caving of the M2 goaf. Therefore, the paroxysmal caving characteristics of the M2 goaf were intense and irregular from July 22, 2019 to December 10, 2019.

It is difficult to show the boundary extension of the M2 goaf in the periodicity caving stage due to the lack of the 3D laser scanning results. However, the field investigation shows that the boundary of the M2 goaf has expanded along the direction of the ore body strike until December 29, 2019, when the boundary begins to expand along the direction perpendicular to the ore body strike. Moreover, the monitoring

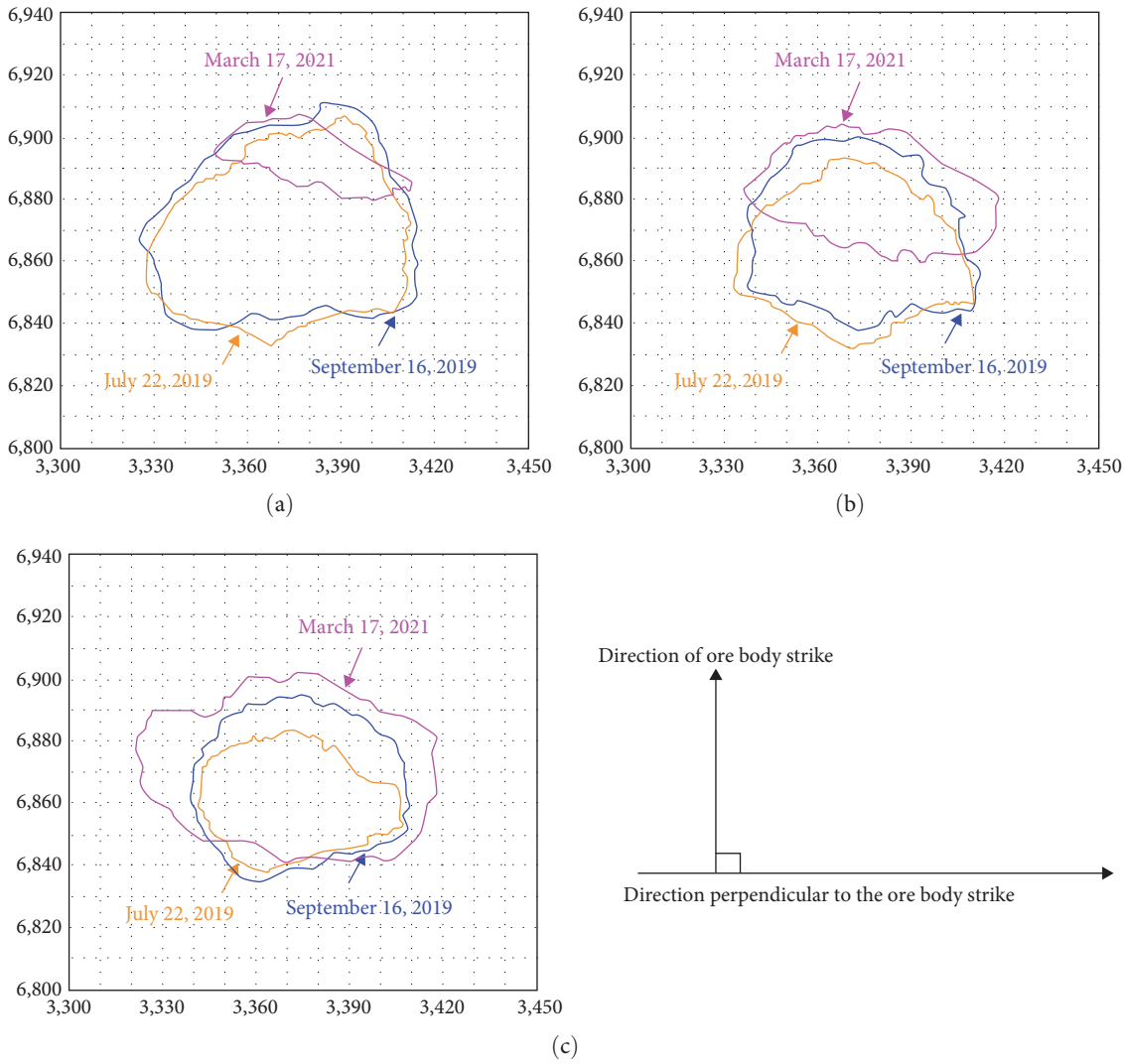

Figure 16: Comparision of the boundary extension of the M2 goaf in the main production level: (a) −210 m level; (b) −195 m level; (c) −180 m level.

results of the crash of the caving rock and the deformation of the arch foot show that the boundary of the M2 goaf in the periodicity caving stage expands along the direction perpendicular to the ore body strike. Therefore, the caving characteristics of the M2 goaf still can be divided into two stages even in the absence of the 3D laser scanning results, and the boundary of M2 goaf in the periodicity caving stage extends along the direction perpendicular to the ore body strike.

It is worth noting that the results of the numerical simulation and the monitoring methods cannot be accurately compared with the results of the 3D laser scanning due to the existence of the multilayer and numerous illegal goaf below the −210 m level. However, the 3D laser scanning results show that the expansion trends of the M2 goaf boundary in two stages are consistent with the results in this work.

According to the recording video obtained from the site, the louder crash sound accompanied by the paroxysmal boom of high and low is dull, rich, and loud, and the average time of a louder crash sound is about 5 min, which conforms to the characteristics of the mass caving of goaf surrounding rock. The deformation monitoring results show that the failure of the arch foot in the deformation monitoring area occurs before the mass caving of the goaf surrounding rock in the periodicity caving stage. Therefore, the deformation of the arch foot can be regarded as a precursor to predict the occurrence time of the goaf mass caving.

Considering that the arch foot deformation is mainly reflected in the expansion of the goaf boundary along the perpendicular to the direction of one body strike, the parameter h_d can be defined as the difference between the two boundary expansions to represent the degree of arch foot deformation. The parameter h_d refers to the difference of the goaf boundary expansion caused by two consecutive cavings in the same roadway, which can be obtained by the laser range finder.

The boundary extension range of M2 goaf in the deformation monitoring area is shown in Figure 17. The values of the parameter h_d and the occurrence time of the goaf boundary expansion are different in the deformation monitoring areas. As shown in Figure 17, the value interval of two

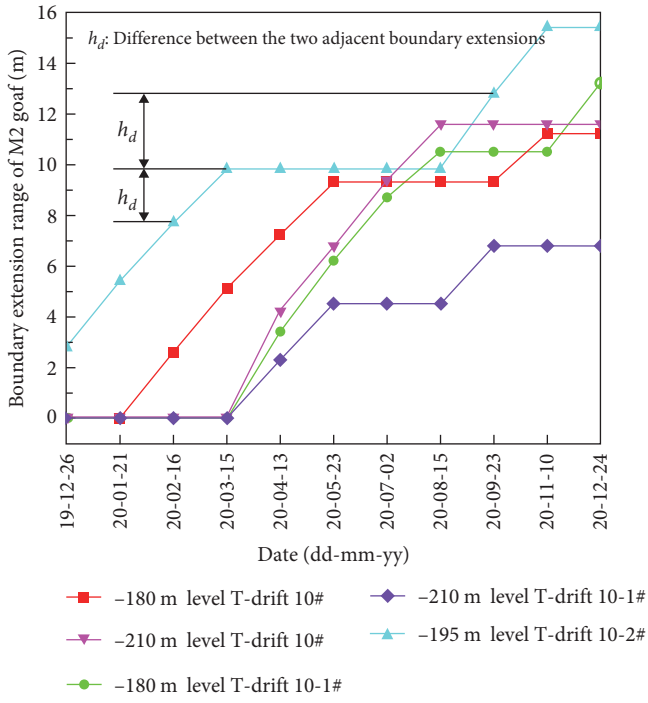

FIGURE 17: Boundary extension range of M2 goaf in the deformation monitoring areas.

boundary expansion differences h_d is (1.9, 2.8 m), the average value is 2.35 m, and the minimum value can be approximated as 2 m. Therefore, the goaf surrounding rock is possible to occur with the mass caving when the boundary extension value of goaf exceeds 2 m in the periodicity caving stage.

The occurrence time of the goaf mass caving in this work is proposed by the relationship between the failure of the arch foot and the goaf mass caving. The peculiarity of the M2 goaf in the Shirengou Iron Mine is large depth, large scale, and irregularity. Moreover, the distribution of lower illegal goaf cannot be clearly detected due to the limitation of the range of mining rights. Then, the goaf arch foot is easily failure by the undiscovered illegal goaf upward caving. Therefore, the applicability of the occurrence time of the mass caving of goaf remains to be further studied due to the large differences in engineering problems.

6. Conclusions

The irregular M2 goaf in the Shirengou Iron Mine has the characteristics of large depth, large scale, undiscovered bottom goaf, intense caving activity, and being located in the main production area. In the process of filling treatment, the surrounding rock caving in the irregular goaf can be divided into two stages: paroxysmal caving and periodicity caving. The caving activity in the paroxysmal caving stage is intense and irregular due to the slow filling speed. Meanwhile, the expansion of the M2 goaf boundary is mainly along the roof and the direction of the ore body strike. The transverse expansion enlarges the span of the goaf and makes the rock movement of the goaf complex and changeable. The periodicity caving stage occurs after the stable state formed by the paroxysmal caving. Meanwhile, the M2 goaf boundary begins to develop along the perpendicular to the direction of the ore body strike. Using the monitoring of the crash of caving rock, the smaller crash sound can characterize the goaf sporadic caving, and the louder crash sound can characterize the goaf mass caving.

The goaf mass caving and the temporary stability of the M2 goaf change periodically alternately in the periodicity caving stage. The interval period of the goaf mass caving is about 15–30 days. Meanwhile, the goaf mass caving occurs after the failure of the arch foot. The lag time for the goaf mass caving is about 3–8 days. Therefore, the deformation of the arch foot may be regarded as a precursor to predict the occurrence time of the goaf mass caving. The mass caving for the M2 goaf surrounding rock occurs when the deformation value exceeds 2 m. Further measurements and observations contribute to the applicability of deformation value due to the differences in engineering problems.

Data Availability

The data used to support the findings of this study are available from the corresponding author upon request.

Conflicts of Interest

The authors declare that they have no conflicts of interest.

Authors' Contributions

Junyang Zhang and Zonghong Zhou contributed to the formulation of the overarching research goals and aims. Junyang Zhang contributed to the numerical simulation. Zonghong Zhou and Jing Zhang were responsible for the monitoring part of the manuscript. Jing Zhang wrote the manuscript, and Junyang Zhang checked the manuscript. Yin Liu and Yang Liu contributed to the collection of test data and references.

Acknowledgments

The support of the National Natural Science Foundation of China (Grant no. 51864023, Grant no. 52264019, Grant no. 51264018), the Yunnan Major Scientific and Technological Projects (Grant no. 202202AG050014), and the Hubei Key Laboratory for Efficient Utilization and Agglomeration of Metallurgic Mineral Resources Open Foundation of China (NO. 2022zy002) is gratefully acknowledged.

References

[1] H. Ding, G. Li, X. Dong, and Y. Lin, "Prediction of pillar stability for underground mines using the stochastic gradient boosting technique," *IEEE Access*, vol. 6, pp. 69253–69264, 2018.

[2] R. Kumar, A. J. Das, P. K. Mandal, R. Bhattacharjee, and S. Tewari, "Probabilistic stability analysis of failed and stable

cases of coal pillars," *International Journal of Rock Mechanics and Mining Sciences*, vol. 144, no. 12, Article ID 104810, 2021.

[3] L. Chuang, L. Huamin, and J. Dongjie, "Numerical simulation study on the relationship between mining heights and shield resistance in longwall panel," *International Journal of Mining Science and Technology*, vol. 27, no. 2, pp. 293–297, 2017.

[4] P. Li, H. Zou, F. Wang, and H. Xiong, "An analytical mechanism of limit support pressure on cutting face for deep tunnels in the sand," *Computers and Geotechnics*, vol. 119, no. 4, Article ID 103372, 2020.

[5] R. Rafiee, M. Ataei, R. Khalokakaie, S. M. E. Jalali, and F. Sereshki, "Determination and assessment of parameters influencing rock mass cavability in block caving mines using the probabilistic rock engineering system," *Rock Mechanics and Rock Engineering*, vol. 48, no. 3, pp. 1207–1220, 2015.

[6] J.-W. Zhang, J.-C. Wang, W.-J. Wei, Y. Chen, and Z.-Y. Song, "Experimental and numerical investigation on coal drawing from thick steep seam with longwall top coal caving mining," *Arabian Journal of Geosciences*, vol. 11, no. 5, pp. 1–19, Article ID 96, 2018.

[7] K. Ding, F. Ma, J. Guo, H. Zhao, R. Lu, and F. Liu, "Investigation of the mechanism of roof caving in the Jinchuan Nickel Mine, China," *Rock Mechanics and Rock Engineering*, vol. 51, no. 4, pp. 1215–1226, 2018.

[8] Haiying, F.-Y. Ren, Y. Zhao, and S. Ren, "Determination of the critical span for a large-caving above a mined-out area Multidisciplinary Sciences," *Current Science*, vol. 116, no. 4, pp. 654–660, 2019.

[9] H. Chen, C. C. Wan, S. G. Zhang, and B. R. Zhou, "In-situ fracturing induced caving of a hard orebody and its application," *Geotechnical and Geological Engineering*, vol. 37, no. 4, pp. 2303–2313, 2019.

[10] K. Yu, C. Zheng, and F. Ren, "Numerical experimental study on ore dilution in sublevel caving mining," *Mining, Metallurgy & Exploration*, vol. 38, no. 1, pp. 457–469, 2021.

[11] K. Xia, C. Chen, T. Wang, K. Yang, and C. Zhang, "Investigation of mining-induced fault reactivation associated with sublevel caving in metal mines," *Rock Mechanics and Rock Engineering*, vol. 55, no. 10, pp. 5953–5982, 2022.

[12] C. Zhang, S. Tu, and Y. X. Zhao, "Compaction characteristics of the caving zone in a longwall goaf: a review," *Environmental Earth Sciences*, vol. 78, no. 1, Article ID 27, 2019.

[13] G.-F. Ren, H.-Y. Yang, S.-S. Zhang, J.-L. Lv, and Z.-L. Song, "On the propagation rules and safety precautions of the air shock waves caused by the roof caving in gypsum mine gob," *Chinese Jounal of Safety and Environment*, vol. 15, no. 6, pp. 86–91, 2015.

[14] X. Ji, P. Ni, M. Barla, W. Zhao, and G. Mei, "Earth pressure on shield excavation face for pipe jacking considering arching effect," *Tunnelling and Underground Space Technology*, vol. 72, pp. 17–27, 2018.

[15] J. Li, Z. Q. Yin, Y. Li, and C. M. Li, "Waste rock filling in fully mechanized coal mining for goaf-side entry retaining in thin coal seam," *Arabian Journal of Geosciences*, vol. 12, no. 16, pp. 1–11, 2019.

[16] D. Zhang, J. Wang, S. Guo, and J. Cao, "Numerical simulation of crack evolution mechanism and subsidence characteristics effected by rock mass structure in block caving mining," *Geotechnical and Geological Engineering*, vol. 40, no. 11, pp. 5377–5395, 2022.

[17] Y. Deng, C. Chen, K. Xia, K. Yang, C. Sun, and X. Zheng, "Investigation on the characteristics of overlying strata caving in the Chengchao Iron Mine, China," *Environmental Earth Sciences*, vol. 77, no. 10, Article ID 362, 2018.

[18] X. Zhao and Q. Zhu, "Analysis of the surface subsidence induced by sublevel caving based on GPS monitoring and numerical simulation," *Natural Hazards*, vol. 103, no. 3, pp. 3063–3083, 2020.

[19] J. Zhao and H. Konietzky, "Numerical analysis and prediction of ground surface movement induced by coal mining and subsequent groundwater flooding," *International Journal of Coal Geology*, vol. 229, Article ID 103565, 2020.

[20] M. G. Karfakis, C. H. Bowman, and E. Topuz, "Characterization of coal-mine refuse as backfilling material," *Geotechnical and Geological Engineering*, vol. 14, no. 2, pp. 129–150, 1996.

[21] M. Li, J. Zhang, N. Zhou, and Y. Huang, "Effect of particle size on the energy evolution of crushed waste rock in coal mines," *Rock Mechanics and Rock Engineering*, vol. 50, no. 5, pp. 1347–1354, 2017.

[22] A. K. Gupta and B. Paul, "A review on utilisation of coal mine overburden dump waste as underground mine filling material: a sustainable approach of mining," *International Journal of Mining and Mineral Engineering*, vol. 6, no. 2, pp. 172–186, 2015.

[23] F. Ren, D. Zhang, J. Cao, M. Yu, and S. Li, "Study on the rock mass caving and surface subsidence mechanism based on an in-situ geological investigation and numerical analysis," *Mathematical Problems in Engineering*, vol. 2018, Article ID 6054145, 18 pages, 2018.

[24] F. Y. Ren, J. Zhang, and Y. Liu, "Study on safe and efficient recovery technology of residual ore in lishugou iron mine," *Chinese Jounal of Metal Mine*, vol. 3, pp. 23–27, 2020.

[25] R. X. He, F. Y. Ren, and D. L. Song, "Induced caving rule of inclined thick ore body in Hemushan iron mine Chinese," *Jounal of Mining and Safety Engineering*, vol. 34, no. 5, pp. 899–904, 2017.

[26] G. Cheng, T. Ma, C. Tang, H. Liu, and S. Wang, "A zoning model for coal mining-induced strata movement based on microseismic monitoring," *International Journal of Rock Mechanics and Mining Sciences*, vol. 94, pp. 123–138, 2017.

[27] V. Palchik, "Experimental investigation of apertures of mining-induced horizontal fractures," *International Journal of Rock Mechanics and Mining Sciences*, vol. 47, no. 3, pp. 502–508, 2010.

[28] G. S. P. Singh and U. K. Singh, "Numerical modeling study of the effect of some critical parameters on caving behavior of strata and support performance in a longwall working," *Rock Mechanics and Rock Engineering*, vol. 43, no. 4, pp. 475–489, 2010.

[29] W. Sui, Y. Hang, L. Ma et al., "Interactions of overburden failure zones due to multiple-seam mining using longwall caving," *Bulletin of Engineering Geology and the Environment*, vol. 74, no. 3, pp. 1019–1035, 2015.

[30] M. Rezaei, "Development of an intelligent model to estimate the height of caving–fracturing zone over the longwall gobs," *Neural Computing and Applications*, vol. 30, no. 7, pp. 2145–2158, 2018.

[31] A. Lannuzzo, A. D. Endice, T. V. Mele, and P. Block, "Numerical limit analysis-based modelling of masonry structures subjected to large displacements," *Computers & Structures*, vol. 242, no. 2, Article ID 106372, 2021.

[32] Z. Ouyang and D. Elsworth, "Evaluation of groundwater flow into mined panels," *International Journal of Rock Mechanics and Mining Sciences & Geomechanics Abstracts*, vol. 30, no. 2, pp. 71–79, 1993.

[33] Z. Yang, Y. Jiang, B. Li, Y. Gao, X. Liu, and Y. Zhao, "Study on the mechanism of deep and large fracture propagation and transfixion in karst slope under the action of mining," *Chinese Jounal of Geomechaics*, vol. 26, no. 4, pp. 459–470, 2020.

[34] B. H. Tan, Z. G. Zhang, and X. M. Chen, "Study on instability mechanism and roof caving mode of downward stratified cemented filling stope," *Chinese Journal of Underground Space and Engineering*, vol. 17, no. 6, pp. 1988–1996, 2021.

[35] J. Zhang, R. He, F. Ren, and Z. Ouyang, "Dimensionless charts for predicting the range of goaf roof caving," *Mathematical Problems in Engineering*, vol. 2021, Article ID 7382550, 14 pages, 2021.

[36] Z.-Q. Luo, J.-J. Huang, Z.-Y. Luo, W. Wang, and Y.-G. Qin, "Integration system research and development for three-dimensional laser scanning information visualization in goaf," *Transactions of Nonferrous Metals Society of China*, vol. 26, no. 7, pp. 1985–1994, 2016.

[37] X. Ba, L. Li, J. Wang et al., "Near-surface site investigation and imaging of karst cave using comprehensive geophysical and laser scanning: a case study in Shandong, China," *Environmental Earth Sciences*, vol. 79, no. 12, Article ID 298, 2020.

[38] K. Wang, J. Qian, H. Zhang, J. Gao, D. Bi, and N. Gu, "Seismic imaging of mine tunnels by ambient noise along linear arrays," *Journal of Applied Geophysics*, vol. 203, Article ID 104718, 2022.

[39] L. Hao, N. Li, X. Xu, Q. Zhang, L. Chen, and F. Sun, "Detecting goaf ahead of the mine tunnel using SAP: a case study in iron mine, China," *Geotechnical and Geological Engineering*, vol. 40, no. 2, pp. 883–897, 2022.

[40] K. Zhang, N. Lin, X. Nie et al., "Application of controlled-source audio-frequency magnetotellurics (CSAMT) for goaf detection: a case study in the Fangzi coal mine China," *Arabian Journal of Geosciences*, vol. 15, no. 12, Article ID 1161, 2022.

[41] P. Wang, Q. Wang, Y. Wang, and C. Wang, "Detection of abandoned coal mine goaf in China's ordos basin using the transient electromagnetic method," *Mine Water and the Environment*, vol. 40, no. 2, pp. 415–425, 2021.

[42] K. Cao, "Simulation of electrical resistance tomography in detecting coal mine goaf," *China Mining Magazine*, vol. 27, pp. 254–260, 2018.

[43] T. Qi, F. Zhang, X. Pei, G. Feng, and H. Wei, "Simulation research and application on response characteristics of detecting water-filled goaf by transient electromagnetic method," *International Journal of Coal Science & Technology*, vol. 9, no. 1, Article ID 17, 2022.

[44] Y. Wang, G. Zheng, and X. Wang, "Development and application of a goaf-safety monitoring system using multi-sensor information fusion," *Tunnelling and Underground Space Technology*, vol. 94, Article ID 103112, 2019.

[45] W. Liu, J. Chen, Y. Luo et al., "Long-term stress monitoring and in-service durability evaluation of a large-span tunnel in squeezing rock," *Tunnelling and Underground Space Technology*, vol. 127, Article ID 104611, 2022.

[46] J. X. Wang, S. B. Tang, M. J. Heap, C. A. Tang, and L. X. Tang, "An auto-detection network to provide an automated real-time early warning of rock engineering hazards using microseismic monitoring," *International Journal of Rock Mechanics and Mining Sciences*, vol. 140, Article ID 104685, 2021.

[47] X. Zhang, W. Zhang, and J. Zhang, "Detecting and locating microseismic events with stacking velocity analysis for surface monitoring," *Journal of Applied Geophysics*, vol. 195, Article ID 104470, 2021.

[48] J. P. Liu, S. D. Xu, and Y. H. Li, "Analysis of rock mass stability according to power-law attenuation characteristics of acoustic emission and microseismic activities," *Tunnelling and Underground Space Technology*, vol. 83, pp. 303–312, 2018.

[49] Z. He, K. Zhao, Y. Yan, F. Ning, Y. Zhou, and Y. Song, "Mechanical response and acoustic emission characteristics of cement paste backfill and rock combination," *Construction and Building Materials*, vol. 288, Article ID 123119, 2021.

[50] L. Han, X. Y. He, and K. S. Liang, "Mining influence law of working face based on microseismic stress joint monitoring," *Chinese Journal of Hunan University of Science and Technology (Natural Science Edition)*, vol. 37, no. 2, pp. 13–17, 2022.

[51] X. Wang, P. Jiang, S. Yan, S. Zhan, R. Huangfu, and S. Wang, "Experimental study on combined acoustic emission and deformation field monitoring," *China Mining Magazine*, vol. 30, no. 2, pp. 203–208, 2021.

[52] H. Fan, T. Li, Y. Gao, K. Deng, and H. Wu, "Characteristics inversion of underground goaf based on InSAR techniques and PIM," *International Journal of Applied Earth Observation and Geoinformation*, vol. 103, 2021.